Klein tunneling in pn and npn junctions of silicene

Ai Yamakage,[1] Motohiko Ezawa,[2] Yukio Tanaka,[1] and Naoto Nagaosa[2,3]

[1]*Department of Applied Physics, Nagoya University, Nagoya 464-8603, Japan*
[2]*Department of Applied Physics, University of Tokyo, Tokyo 113-8656, Japan*
[3]*RIKEN Center for Emergent Matter Science, ASI, RIKEN, Wako, Saitama 351-0198, Japan*

(Dated: March 27, 2013)

We investigate Klein tunneling of pn and npn junctions made from silicene, Si analogue of graphene. The conductance shows the distinct gate-voltage dependences peculiar to the topological and non-topological phases, where the topological phase transition is caused by external electric field. Namely, the conductance is suppressed in the np regime when the both sides are topological, while in the nn regime when one side is topological and the other side is non-topological. Furthermore, we find that the conductance is almost quantized to 0, 1 and 2. Hence we can use a silicene pn junction as a digital field-effect transistor. Our findings will open a new nanoelectronics based on silicene.

PACS numbers: 73.23.-b, 72.80.Vp,73.40.-c

I. INTRODUCTION

Technology fabricating one-atom thick systems has been rapidly developing since the appearance of monolayer honeycomb carbon (graphene).[1] Recently, Si analog of graphene (silicene)[2–4] has been synthesized. The low-lying excitations of the monolayer honeycomb systems are Dirac fermions. Due to spin-orbit interaction (SOI), the Dirac fermions become massive, i.e., the energy bands have a gap. These massive Dirac fermion systems lead to a quantum spin Hall (QSH) insulator, which is originally proposed in a graphene.[5,6] Unfortunately, SOI of graphene is tiny so that the QSH effect in a graphene has not been experimentally observed. SOI of silicene is, in contrast, thousand times larger than that of graphene.[7,8] The QSH effect in silicene is experimentally accessible.[9]

Transport of Dirac fermions shows various anomalous behaviors. A massless Dirac fermion never shows localization[10] owing to the topological term.[11] Furthermore, Klein tunneling occurs in Dirac fermions.[12] Especially, for the massless case, a perfect transmission through any barrier potential occurs.[13,14] This originates from the topological phase (Berry phase) π.[15] It is difficult to observe the Klein tunneling for elementary particles, due to a huge mass gap. In contrast, it is possible for semiconductors in which the band gap is small ($\sim$ 1eV). Actually, the Klein tunneling has been observed in graphene.[16] The topologically protected transport is robust against perturbations. Thus, the systems supporting Dirac fermions can exhibit unique charge and spin transport. They have a potential to be a new electronics and spintronics device.

Among such Dirac fermion systems, silicene has another advantage: the band gap is controllable by applying an external electric field[17] owing to the buckling structure.[18] A bilayer graphene also has an electric-field-tunable band gap.[19–23] Silicene, differently from a bilayer graphene, shows the topological phase transition with tuning the band gap. If one applies an electric field whose energy is stronger than SOI, the topological phase transition from a QSH to non-topological insulators occurs. Also, silicene realizes various topological insulators by exchange interaction,[24] photo-irradiation[25] and antiferromagnetic order.[26]

These characteristics can be useful for device applications. The most fundamental electronic device is a field-effect transistor (FET). FET made by silicene has an advantage that it has a large band gap due to SOI compared with graphene which is a zero gap semiconductor. In addition, the tunable band gap and the topological phase transition of silicene by external electric field may lead to a new feature for FETs.

Charge transport properties of a silicene nanoribbon has been studied.[27] Spin transport has been also studied in a bulk silicene junction under Zeeman field.[28] On the other hand, we focus on the charge transport in the bulk silicene. In this paper, we analyze the transport properties of pn and pnp junctions made of silicene. Controlling the conductance by tuning the gate voltage, we find that i) the gate-voltage dependences of conductance in the topological and non-topological phases are quite distinct, and ii) the conductance is almost quantized to 0, 1 and 2. The former is an evidence for the existence of the topological phase. The latter enables us to use silicene as a FET with three digital values of conductance. Our results will open a new way to future nanoelectronics.

This paper is composed as follows. In Sec. II, we review the bulk properties of silicene. In Sec. III, we investigate the pn junction of silicene. First we calculate the one-dimensional model with and without the Rashba interaction. Next we calculate the two-dimensional model. The conductance of the two-dimensional model is almost the same but smeared compared with that of the one-dimensional model. In sec. IV, we investigate a pnp junction of silicene. Section V is devoted to discussions.

II. BULK PROPERTIES

First, we show the bulk properties of silicene. Hamiltonian of a silicene in the vicinity of the K and K′ points reads[9,17,29]

$$H(\boldsymbol{k}) = \hbar v_{\rm F}(k_x\tau_x - k_y\tau_y\eta_z) - \lambda_{\rm SO}\tau_z\sigma_z\eta_z + a\lambda_{\rm R}\tau_z(k_x\sigma_y - k_y\sigma_x)\eta_z + \ell E_z\tau_z, \quad (1)$$

where σ_i, τ_i, and η_i are the Pauli matrices for the spin ($\uparrow$ and $\downarrow$), sublattice (A and B sites) pseudospin, and valley (K and K′ points) spaces, respectively. a denotes the lattice constant. $\lambda_{\rm SO}$ is the intrinsic SO coupling constant that triggers the topological phase transition from the non-topological to topological insulators (See below). The sublattice-dependent Rashba SO interaction $\lambda_{\rm R}$ also appears due to the buckling structure of silicene. And also, the mass term $\ell E_z\tau_z$ shows up because of the buckling structure with an external electric field E_z along the z-axis. Hereafter, we set $\hbar = 1$.

Here we review the topological phase diagram of silicene. The Dirac mass m for the K point ($\eta_z = 1$) in the bulk silicene is given by

$$m = -\lambda_{\rm SO}\tau_z\sigma_z + \ell E_z\tau_z. \quad (2)$$

The system is a topological insulator for $\lambda_{\rm SO} > \ell|E_z|$, while it is a non-topological insulator for $\lambda_{\rm SO} < \ell|E_z|$. $\lambda_{\rm SO} = \ell|E_z|$ is the critical point, where the energy gap closes. The sign-change of the mass term means inversion between the conduction and valence bands. Correspondingly, direction of $\boldsymbol{\tau}$ and $\boldsymbol{\sigma}$ of the conduction and valence electrons changes. Namely, the sublattice and spin states is given by $|{+}{-}\rangle$, $|{-}{-}\rangle$, $|{+}{+}\rangle$, and $|{-}{+}\rangle$ in descending energy order for the topological phase. On the other hand, the second and third states are interchanged for the non-topological phase, i.e., $|{+}{-}\rangle$, $|{+}{+}\rangle$, $|{-}{-}\rangle$, and $|{-}{+}\rangle$. Here $|\alpha\beta\rangle$ denotes the eigenstate with $\tau_z = \alpha\,\mathrm{sgn}(E_z)$ and $\sigma_z = \beta\,\mathrm{sgn}(E_z)$. This energy level scheme is shown in Fig. 1. As one switches off E_z, the two states with $|{+}{-}\rangle$ and $|{-}{-}\rangle$ (with $|{+}{+}\rangle$ and $|{-}{+}\rangle$) are degenerated ($\epsilon_1 = \epsilon_2$ in Fig. 1).

In addition, we show the energy dispersions for $E_z = 0$ and $E_z \neq 0$ in Fig. 2. The energy $E_\pm(\boldsymbol{k})$ in the bulk is obtained to be

$$E_\pm^2(\boldsymbol{k}) = v_{\rm F}^2k^2 + \left(\pm\sqrt{\lambda_{\rm SO}^2 + a^2\lambda_{\rm R}^2k^2} + \ell E_z\right)^2, \quad (3)$$

with $k = (k_x^2 + k_y^2)^{1/2}$. The corresponding eigenvector $\boldsymbol{u}_\pm(\boldsymbol{k}; E_z)$ is also obtained analytically (Appendix A). The energy bands are doubly degenerated for $E_z = 0$ due to the inversion $[\tau_z\sigma_z H(\boldsymbol{k})\sigma_z\tau_z = H(-\boldsymbol{k})]$ and time-reversal $[\tau_y\sigma_x H^*(\boldsymbol{k})\sigma_x\tau_y = H(-\boldsymbol{k})]$ symmetries defined within each valley. In contrast, there is no spin-degeneracy for $E_z \neq 0$ since E_z breaks the time-reversal symmetry defined within each valley.

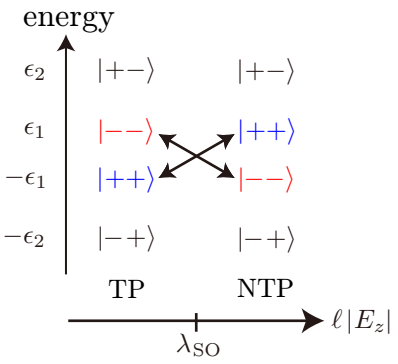

FIG. 1. Energy level scheme for the topological (TP) ($\ell\,|E_z| < \lambda_{\rm SO}$) and non-topological (NTP) ($\ell\,|E_z| > \lambda_{\rm SO}$) phases at the K point. $|\alpha\beta\rangle$ denotes the eigenstate with $\tau_z = \alpha\,\mathrm{sgn}(E_z)$ and $\sigma_z = \beta\,\mathrm{sgn}(E_z)$. $\epsilon_1 = \lambda_{\rm SO} + \ell\,|E_z|$, $\epsilon_2 = |\lambda_{\rm SO} - \ell\,|E_z||$.

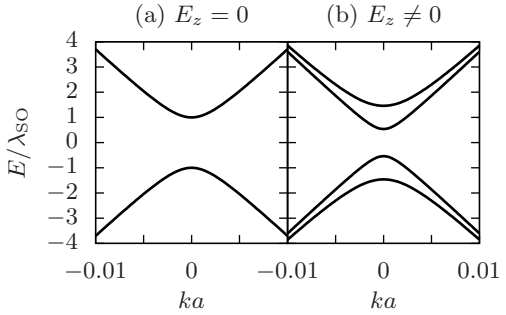

FIG. 2. Energy dispersions in the bulk silicene for $E_z = 0$ (a) and $E_z = 0.5\lambda_{\rm SO}$ (b). The parameters of the system are taken as follows. $v_{\rm F}/a = 1.4$eV, $\lambda_{\rm SO} = 3.9$meV, $\lambda_{\rm R} = 0.7$meV.

III. SILICENE PN JUNCTION

In this section, we investigate a charge transport in a silicene pn junction, which is illustrated in Fig. 3.

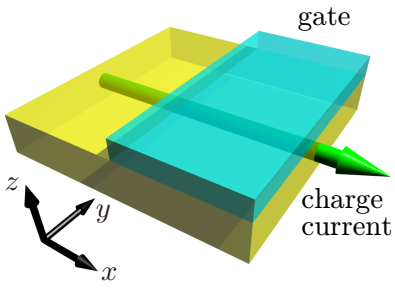

FIG. 3. Schematic of a pn junction.

A. One–dimensional case

1. Formalism of the scattering problem

Firstly, we consider a pn junction of one-dimensional silicene. The Hamiltonian is given by

$$H(x) = -iv_{\rm F}\partial_x\tau_x - \lambda_{\rm SO}\tau_z\sigma_z\eta_z + \ell E_z\theta(x)\tau_z + ia\lambda_{\rm R}\partial_x\sigma_y\tau_z\eta_z + V\theta(x). \quad (4)$$

Hereafter, we focus only on the K point ($\eta_z = 1$). The same analysis is applicable to the K′ point.

We solve the scattering problem of the pn junction. The calculation is done by employing theories for graphene[13,14,30] and the Kane-Mele model.[31,32] In the incident side ($x < 0$), an external electric field is not applied and hence the energy bands are doubly degenerated. As a result, there are two incident states for a fixed incident energy $E_{\rm F}$. Wave function $\psi_\pm(x)$ of the scattering state with the incident energy being $E_{\rm F}$ has the form as

$$\psi_\pm(-0) = \boldsymbol{u}_\pm(k_{\rm I};0) + r_{\pm+}\boldsymbol{u}_+(-k_{\rm I};0) + r_{\pm-}\boldsymbol{u}_-(-k_{\rm I};0), \quad (5)$$

$$\psi_\pm(+0) = t_{\pm+}\boldsymbol{u}_+(q_+;E_z) + t_{\pm-}\boldsymbol{u}_-(q_-;E_z), \quad (6)$$

where the subscript of $\psi_\pm(x)$ denotes the spin state of the incident state $\boldsymbol{u}_\pm(k_{\rm I};0)$. The first term $\boldsymbol{u}_\pm(k_{\rm I};0)$ of Eq. (5) denotes the incident state. The other two terms correspond to the reflected states with the same ($\pm$) and different (spin-flip, $\mp$) spin states. Momentum $k_{\rm I}$ of the incident electron is given by

$$k_{\rm I} = {\rm sgn}(E_{\rm F})\sqrt{\frac{E_{\rm F}^2 - \lambda_{\rm SO}^2}{v_{\rm F}^2 + a^2\lambda_{\rm R}^2}}. \quad (7)$$

The sign of $k_{\rm I}$ is determined so that the group velocity of the incident state is positive. Note that the incident state must be a propagating mode; $E_{\rm F}^2 > \lambda_{\rm SO}^2$. Otherwise, the corresponding conductance is zero, by definition. On the other hand, momentum $q_\pm$ of the transmitted electron is obtained by solving the following equation;

$$(E_{\rm F} - V)^2 = v_{\rm F}^2 q_\pm^2 + \left(\pm\sqrt{\lambda_{\rm SO}^2 + a^2\lambda_{\rm R}^2 q_\pm^2} + \ell E_z\right)^2. \quad (8)$$

Since the group velocities of the transmitted electrons should be positive, the following relation is satisfied for the propagating mode;

$${\rm sgn}\left(q_\pm\right) = {\rm sgn}\left(E_{\rm F} - V\right). \quad (9)$$

For the evanescent mode, on the other hand, ${\rm Im}\, q_\pm > 0$ is satisfied. And note that when $|E_{\rm F} - V| < |\lambda_{\rm SO} - \ell\,|E_z||$, the system in $x > 0$ becomes insulating, i.e., the resulting conductance vanishes.

The reflection and transmission coefficients $r_{\pm\pm}$ and $t_{\pm\pm}$ are obtained by solving the continuity condition at $x = 0$. Since charge current is conserved, the following relation holds.

$$\left.\frac{\partial H}{\partial(-i\partial_x)}\right|_{x<0}\psi_\pm(-0) = \left.\frac{\partial H}{\partial(-i\partial_x)}\right|_{x>0}\psi_\pm(+0), \quad (10)$$

where $\partial H/[\partial(-i\partial_x)]$ is the velocity operator. The above relation is reduced to

$$\psi_\pm(-0) = \psi_\pm(+0). \quad (11)$$

Solving this, one obtains the reflection and transmission coefficients. From the reflection coefficient $r_{\alpha\beta}$, the transmission probability $T_\pm$ is given by

$$T_\pm = 1 - \sum_{\beta=\pm}|r_{\pm\beta}|^2. \quad (12)$$

Charge conductance G in the one-dimensional system is defined by

$$G = \frac{e^2}{h}(T_+ + T_-). \quad (13)$$

2. Charge transport asymmetry in the nn and pn regimes

We show results on the conductance of the one-dimensional pn junction in Fig. 4. The horizontal axis is $(E_{\rm F} - V)/E_{\rm F}$, where $E_{\rm F} - V$ corresponds to the Fermi energy in $x > 0$ measured from the charge neutrality point. The vertical axis is $\ell E_z/\lambda_{\rm SO}$. Only the region of $\ell E_z/\lambda_{\rm SO} > 0$ is shown since the transmission probability is symmetric with respect to $E_z = 0$ (See Appendix B). A pn junction with two doped topological insulators (TP/TP) is realized for $\ell|E_z| < \lambda_{\rm SO}$. On the other hand, that with doped topological and non-topological (TP/NTP) insulators is realized for $\ell|E_z| > \lambda_{\rm SO}$. Clearly seen from Fig. 4, there is no qualitative difference between the conductances with [Figs. 4(a) and (b)] and without [Figs. 4(c) and (d)] the sublattice-dependent Rashba SOI $\lambda_{\rm R}$.

For $\lambda_{\rm R} = 0$, one can obtain a simple formula for the reflection coefficient. The reflection coefficient r_σ with $\sigma = \pm$ being the z-component of spin of the incident electron is given by

$$r_\sigma = \frac{1 - X_\sigma}{1 + X_\sigma}, \quad (14)$$

with

$$X_\sigma = \sqrt{\frac{E_{\rm F} + \sigma\lambda_{\rm SO}}{E_{\rm F} - \sigma\lambda_{\rm SO}}\frac{E_{\rm F} - V - \sigma\lambda_{\rm SO} + \ell E_z}{E_{\rm F} - V + \sigma\lambda_{\rm SO} - \ell E_z}}. \quad (15)$$

The conductance is given by $G = (e^2/h)(2 - \sum_\sigma |r_\sigma|^2)$. If $\lambda_{\rm SO} \ll |E_{\rm F}|$ and $\ell|E_z| \ll |E_{\rm F} - V|$, the corresponding r_σ tends to zero, i.e., a perfect transmission occurs, which is known as the Klein tunneling in monolayer graphene.[13,14]

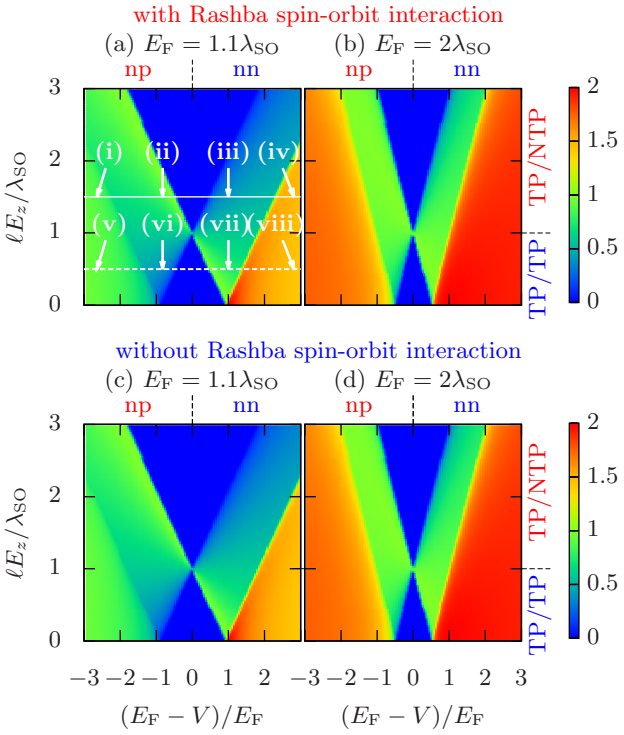

FIG. 4. Conductance in unit of e^2/h for the one-dimensional junction in the presence [(a) and (b)] ($\lambda_R = 0.7$meV) and absence [(c) and (d)] ($\lambda_R = 0$) of the Rashba SOI. (a) and (c) [(b) and (d)] are the lightly (heavily) doped case as $E_F = 1.1\lambda_{SO}$ ($E_F = 2\lambda_{SO}$). The solid and dashed lines in (a) are located at $\ell E_z = 1.5\lambda_{SO}$ and $\ell E_z = 0.5\lambda_{SO}$, respectively. (i)–(viii) are the representative points for which the conductance is shown in Fig. 5. These are defined as follows. (i) and (v): $V = 4\lambda_{SO}$ (np and the double-channel regime). (ii) and (vi): $V = 2\lambda_{SO}$ (np and the single-channel regime). (iii) and (vii): $V = 0$ (nn and the single-channel regime). (iv) and (viii): $V = -2\lambda_{SO}$ (nn and the double-channel regime).

Here we go back to Fig. 4. In the inner region of $|E_F - V| < \epsilon_1 \equiv |\lambda_{SO} - \ell|E_z||$, the conductance vanishes since the transmitted side ($x > 0$) is insulating. In the central region of $\epsilon_1 < |E_F - V| < \epsilon_2 \equiv \lambda_{SO} + \ell|E_z|$, there is a single energy band at the Fermi level, hence the maximum value of resultant conductance is e^2/h. On the other hand, in the outer region of $|E_F - V| > \epsilon_2$, two energy bands are located at the Fermi level. Here the conductance becomes larger (almost double) than that in the central region. We refer to these regions as insulating, single-channel, and double-channel regimes, respectively. This behavior originates from a peculiarity of silicene, i.e., band gap and spin-split energy bands owing to SOI and electric-field effect in the buckling structure. Graphene, in contrast, does not have SOI nor the buckling structure. The resulting conductance is always $2e^2/h$.

For the lightly doped case [$E_F = 1.1\lambda_{SO}$, Figs. 4(a) and 4(c)], one can see asymmetry of the conductance with respect to $\ell E_z = \lambda_{SO}$. To be more explicit we show

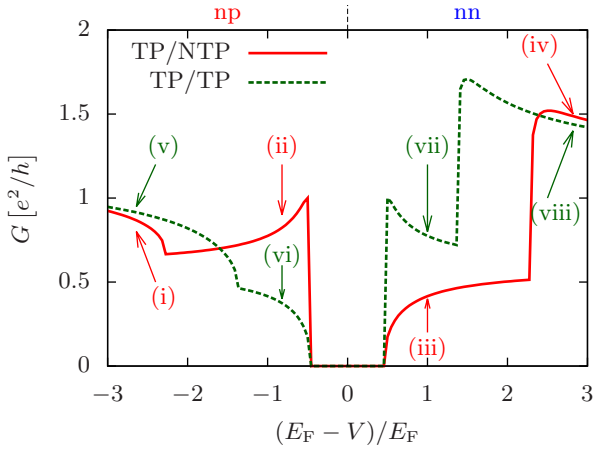

FIG. 5. Conductances for the one-dimensional TP/NTP ($\ell E_z = 1.5\lambda_{SO}$) and TP/TP ($\ell E_z = 0.5\lambda_{SO}$) junctions in the case of normal incidence. The parameters are the same as in Fig. 2. Cases (i)–(viii) correspond to those in Fig. 4(a).

the conductance as a function of V for $E_z = 1.5\lambda_{SO}$ (TP/NTP junction) and $E_z = 0.5\lambda_{SO}$ (TP/TP junction) in Fig. 5. For the double-channel regime ($|E_F - V| > \epsilon_2$) [(i), (iv), (v), and (viii)], the transmission probabilities of the TP/NTP and TP/TP junctions are almost the same. The transmission probability in the nn regime [(iv) and (viii)] is slightly larger than that in the np regime [(i) and (v)]. In contrast, for the single-channel regime ($\epsilon_1 < |E_F - V| < \epsilon_2$) [(ii), (iii), (vi), and (vii)], the conductances of the TP/NTP and TP/TP junctions are qualitatively different. Namely, the conductance for the TP/NTP (TP/TP) junction in the np (nn) regime (ii) [(vii)] takes a larger value than that in the nn (np) regime (iii) [(vi)]. Note that the gate-voltage dependence of the conductance for the TP/NTP junction is distinct to that for the TP/TP junction.

This asymmetric behavior of conductance stems from the sublattice and spin states of the incident and transmitted electrons. Figure 6 shows the energy bands for $x < 0$ and $x > 0$. The sublattice and spin states $|\alpha\beta\rangle$ for each energy band at $k = 0$ are also denoted in Fig. 6. The incident states ($x < 0$) with a positive energy are approximately given by $|+-\rangle$ and $|--\rangle$. When the transmitted states is given by $|--\rangle$ [(ii) and (vii)] or $|+-\rangle$ [(iv) and (viii)], the conductance is large, due to matching of the sublattice and spin states. Especially, for $(E_F - V)/E_F \sim -0.5$ and $(E_F - V)/E_F \sim 0.5$, the transmission probabilities are unity since the sublattice and spin states of the incident and transmitted electrons coincide with each other. In contrast, when the transmitted state is given by the mismatched state $|++\rangle$ [(iii) and (vi)] or $|-+\rangle$ [(i) and (v)], the corresponding conductance is suppressed. Thus the matching/mismatching of the sublattice and spin states gives a larger/smaller conductance.

It is emphasized that the transmitted states $|++\rangle$ and $|--\rangle$ are controlled by E_z. As shown in Fig. 1, the two

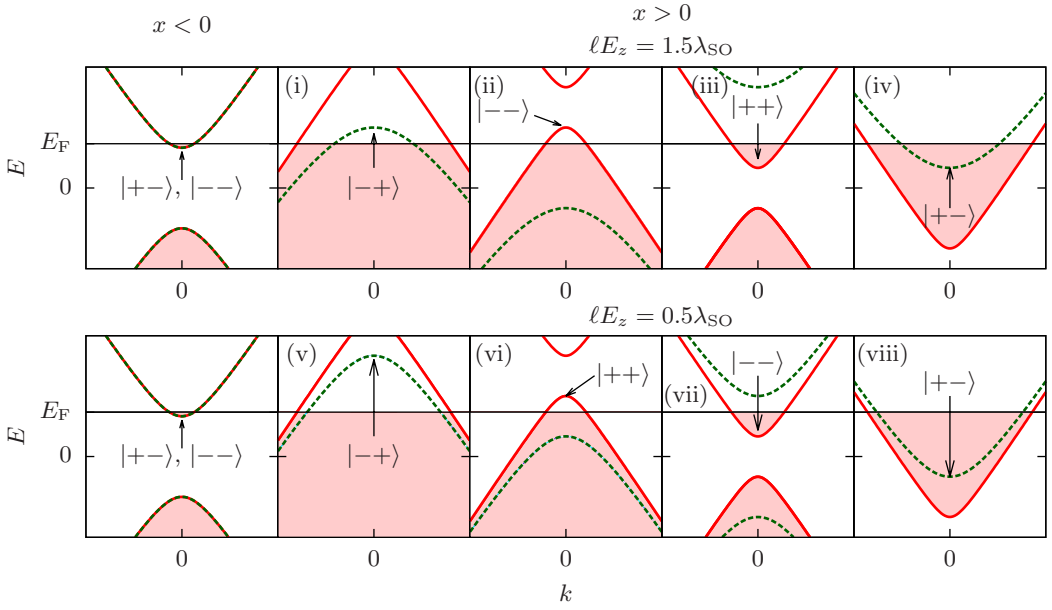

FIG. 6. Energy spectra for the incident ($x < 0$) state with $\ell E_z = 0$ (the left-upper and left-lower panels), and for transmitted ($x > 0$) states with $\ell E_z = 1.5\lambda_{\rm SO}$ [(i)–(iv)] and with $\ell E_z = 0.5$ [(v)–(viii)]. Cases (i)–(viii) corresponds to those in Fig. 4. $|\alpha\beta\rangle$ with $\tau_z = \alpha\,\mathrm{sgn}\,(E_z)$ and $\sigma_z = \beta\,\mathrm{sgn}\,(E_z)$ denotes the sublattice and spin state for $k = 0$.

	np	nn
TP/NTP	large	small
TP/TP	small	large

TABLE I. Magnitudes of conductances in the silicene junctions for the single-channel regime ($\epsilon_1 < |E_{\rm F} - V| < \epsilon_2$). In the junction, the two cases are realized: the gated region is nontopological (TP/NTP) and topological (TP/TP).

states $|++\rangle$ and $|--\rangle$ are interchanged in the different topological phases, which is determined by E_z. In other words, the conductance is highly tuned by E_z through changing the symmetry of the wave function. The obtained results are summarized in Table. I. The same behavior is studied in Ref. 33 on the surface of a topological insulator with ferromagnets.

As explained above, the conductance controlled by E_z stems from the sublattice and spin states, i.e., the Dirac mass term. Therefore, this behavior does not appear in the heavily doped case ($|E_{\rm F}| \gg \lambda_{\rm SO}, \ell\,|E_z|$) [Figs. 4(b) and 4(d)], where the mass gap $\sim \lambda_{\rm SO}$ is negligible as compared to $E_{\rm F}$. The conductance asymmetry peculiar to the topological phase can be expected for other topological insulators, provided that the system has a single Fermi surface in the pn junction.

3. *Digital field-effect transistor*

A heavily doped silicene can be applied to a new electronic device: a silicene pn junction operates as a FET with digital values of conductance. From Figs. 4 (b) and (d), the transmission probability is almost quantized to 0 for the insulating case ($|E_{\rm F} - V| < \epsilon_1$), to 1 for the single-channel regime ($\epsilon_1 < |E_{\rm F} - V| < \epsilon_2$), and to 2 for the double-channel regime ($|E_{\rm F} - V| > \epsilon_2$). This is a consequence of the Klein tunneling of Dirac fermions: A massless Dirac fermion can tunnel through any barriers. And yet the normal incident transmission probability is unity.[13,14] Although silicene has a finite energy gap, a perfect transmission approximately occurs for a heavily doped case, since the energy gap is effectively ignored as compared to the incident energy. In contrast, a graphene pn junction always shows a perfect transmission, i.e., the value of conductance is always $2e^2/h$. Graphene cannot be used as a FET.

B. Two–dimensional case

Next we turn to the two-dimensional case, which corresponds to an actual silicene pn junction. The Hamiltonian of the two-dimensional system in the vicinity of K point reads

$$H(x) = -iv_{\rm F}\partial_x\tau_x - k_y\tau_y - \lambda_{\rm SO}\tau_z\sigma_z + \ell E_z\theta(x)\tau_z - a\lambda_{\rm R}(-i\partial_x\sigma_y - k_y\sigma_x)\tau_z + V\theta(x). \quad (16)$$

Here we assume translational invariance along the y-axis, i.e., the y-component of momentum k_y is regarded as a parameter. We solve the scattering problem in the same way as in the previous section.

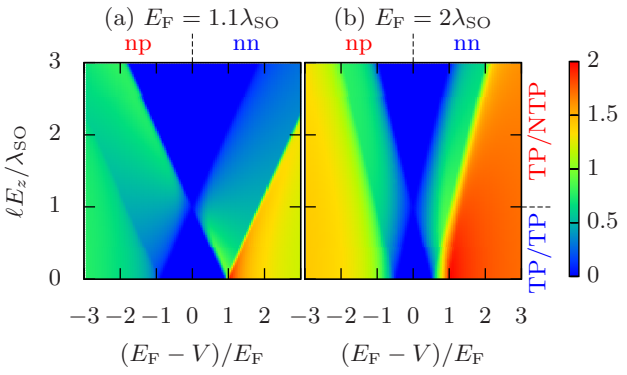

FIG. 7. Normalized conductance G/G_0 averaged over the incident angles for the lightly (a) ($E_F = 1.1\lambda_{SO}$) and the heavily (b) ($E_F = 2\lambda_{SO}$) doped cases.

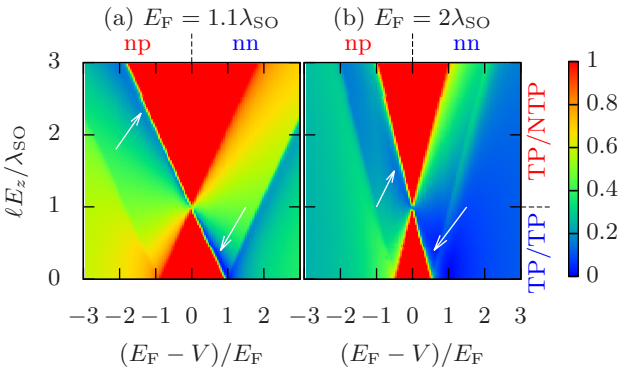

FIG. 8. Fano factor for the lightly (a) ($E_F = 1.1\lambda_{SO}$) and the heavily (b) ($E_F = 2\lambda_{SO}$) doped cases.

The normalized conductance G/G_0 is given by

$$\frac{G}{G_0} = \int_{-\pi/2}^{\pi/2} \frac{d\theta}{2} \cos\theta \, [T_+(\theta) + T_-(\theta)], \tag{17}$$

with $T_\pm(\theta)$ being the transmission probability for an incident angle θ defined by $k_y = k_F \sin\theta$ and for incident spin $\pm$. In the case of perfect transmission ($T_\pm(\theta) = 1$), the resulting conductance takes the value of $G = 2G_0$, where factor 2 means that the system has two incident states $\boldsymbol{u}_+$ and $\boldsymbol{u}_-$ with different spin states. Here, $G_0 = (k_F W/\pi)e^2/h$, $k_F = [(E_F^2 - \lambda_{SO}^2)/(v_F^2 + a^2\lambda_R^2)]^{1/2}$, and W being the width of the system. Also, Fano factor F, which corresponds to the shot noise-to-signal ratio, is given by

$$F = \frac{G_0}{G} \sum_{\alpha=\pm} \int_{-\pi/2}^{\pi/2} \frac{d\theta}{2} \cos\theta \, T_\alpha(\theta) \, [1 - T_\alpha(\theta)] \, . \tag{18}$$

Figure 7 shows the normalized charge conductance G/G_0 as a function of gate voltage $[(E_F - V)/E_F]$ and electric field $(\ell E_z/\lambda_{SO})$. Obviously, the charge conductance of the two-dimensional pn junction (Fig. 7) and the transmission probability of the one-dimensional pn junction [Figs. 4(a) and 4(b)] are almost the same, except for the broadening of line shape. This is because transport is determined basically by the normal incidence. An integral over the incident angle θ solely gives line broadening of the charge conductance from that for the normal incidence $T(\theta = 0)$.

The Fano factor of the two-dimensional junction is shown in Fig. 8. Overall, the resulting Fano factor for the lightly doped case (a) is smaller than that for the heavily doped case (b). Also, the Fano factor is roughly given by the inverse of conductance, i.e., it takes a small (large) value when the corresponding conductance is large (small). This behavior is realized if the shot noise power is almost independent of the parameters (V and E_z). On the other hand, in the single-channel regime, the Fano factor is strongly suppressed when the sublattice and spin states of the incident and transmitted electrons are coincides with each other (denoted by the arrows in Fig. 8). Note that the Fano factor in the insulating region ($|E_F - V| < \epsilon_1$) is obtained to be unity, although it is not well-defined for metal-insulator junctions because the corresponding conductance vanishes ($F \to 0/0$). We have concluded $F = 1$ in the insulating region since $F = 1$ has been obtained for the long junction limit of the npn junction, as discussed in the next section.

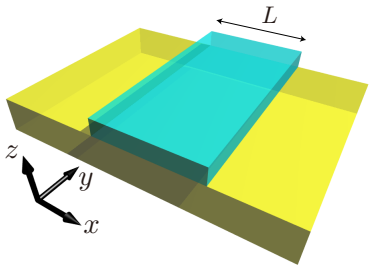

FIG. 9. Silicene npn junction. The center region (the length L) is gated. Charge current flows along the x-axis.

IV. SILICENE NPN JUNCTION

Next we investigate charge transport in a silicene npn junction, where electrostatic field is applied in $0 < x < L$, which is illustrated in Fig. 9. The scattering problem of the npn junction is solved in a manner similar to that of the pn junction. The wave function $\psi_\pm(x)$ is given by

$$\psi_\pm(x = -0) = \boldsymbol{u}_\pm(k_I; 0) + r_{\pm+}\boldsymbol{u}_+(-k_I; 0) + r_{\pm-}\boldsymbol{u}_-(-k_I; 0), \tag{19}$$

$$\psi_\pm(0 < x < L) = \sum_{i=1}^{4} w_{\pm i}\boldsymbol{u}_{\alpha_i}(q_i; E_z)e^{iq_i x}, \tag{20}$$

$$\psi_\pm(x = L + 0) = t_{\pm+}\boldsymbol{u}_+(k_I; 0)e^{ik_I L} + t_{\pm-}\boldsymbol{u}_-(k_I; 0)e^{ik_I L}, \tag{21}$$

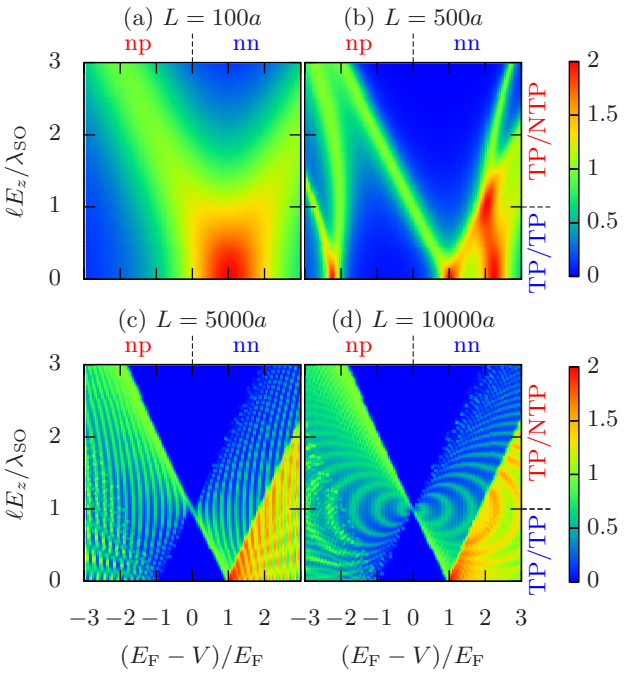

FIG. 10. Conductance in unit of e^2/h for the one-dimensional npn junction ($\theta = 0$). L and a denote the length of the gate in the junction and the lattice constant, respectively. The incident energy is taken to be $E_{\rm F} = 1.1\lambda_{\rm SO}$.

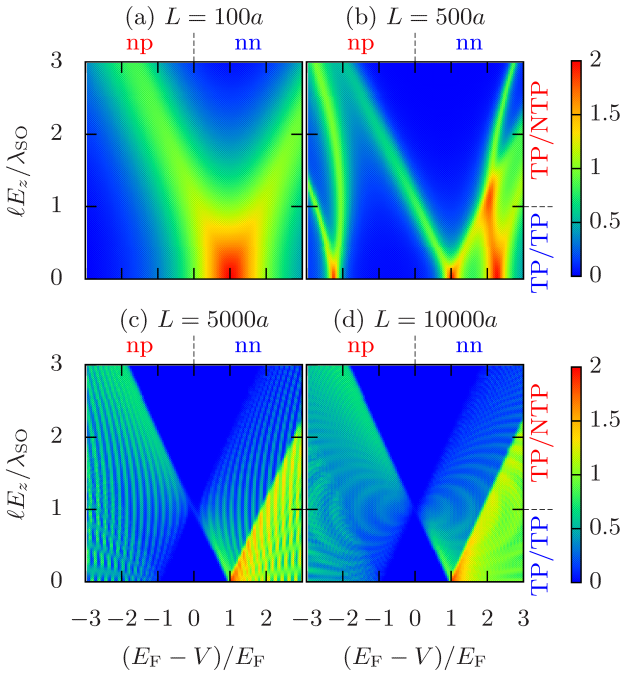

FIG. 11. Normalized Conductance G/G_0 in the two-dimensional npn junction for $E_{\rm F} = 1.1\lambda_{\rm SO}$.

where q_i and α_i are solutions of $E_{\rm F} - V = E_{\alpha_i}(q_i, k_y)$. Coefficients $r_{\pm\pm}$, $w_{\pm i}$, and $t_{\pm\pm}$ are obtained by solving the following boundary condition:

$$\psi_\pm(-0) = \psi_\pm(+0), \tag{22}$$
$$\psi_\pm(L-0) = \psi_\pm(L+0). \tag{23}$$

The normalized conductance and Fano factor are obtained by Eqs. (17) and (18), respectively.

A. One–dimensional case

First we show the conductance for the one-dimensional case in Fig. 10, i.e., $T_+(0) + T_-(0)$. A resonant tunneling occurs for $q_i L = 2n\pi, n \in \mathbb{Z}$ in a npn junction. In the short junction limit ($L \to 0$), a perfect transmission always occurs even when the central region is insulating. In the short but finite-length junction [Fig. 10(a)], the number of resonant peaks ($q_i = 2n\pi/L$) is still small (two peaks). On the other hand, the peak width is broad ($\sim 2\lambda_{\rm SO}$) since the length of the junction is short so that the transmission probability is large. Thus, two broad resonant peaks appear in Fig. 10(a). As one increases L, the number of resonant peaks increases and the peak width becomes narrower, as shown in Figs. 10(b) and 10(c). Finally, the transmission probability of the long junction ($L > 10000a$) [Fig. 10(d)] asymptotically converges to that of the pn junction [Fig. 4(a)].

B. Two–dimensional case

Next we show results on the two-dimensional case. The charge conductance is shown in Fig. 11. As in the case of the pn junction discussed in Sec. III B, integral over the incident angle entirely causes broadening of detail structures in the conductance. Namely, the conductance of the two-dimensional junction [Figs. 11(a)-(d)] is almost the same as that of the one-dimensional junction [Figs. 10(a)-(d)].

In addition, we show the Fano factor of the two-dimensional junction in Fig. 12. The Fano factor (Fig. 12) is basically given by the inverse of G (Fig. 11): F takes a small value for a resonant tunneling case. In the long junction limit [Figs. 12(c) and 12(d)], F of the npn junction tends to that of the pn junction [Fig. 8(a)]. And also, in the insulating regime ($|E_{\rm F} - V| < \epsilon_1$), F converges to be unity. Namely, the Fano factor is interpreted to be unity for the insulating regime of pn junction.

V. SUMMARY

We have studied charge transport in the pn and npn junctions of silicene. In silicene, the topological phase transition occurs by applying electric field owing to the buckling structure. This transition affects the charge transport for the single-channel regime, i.e., the resulting conductance is suppressed in the np regime for the TP/TP junction, while it is suppressed in the nn regime for the TP/NTP junction. We have shown that this sup-

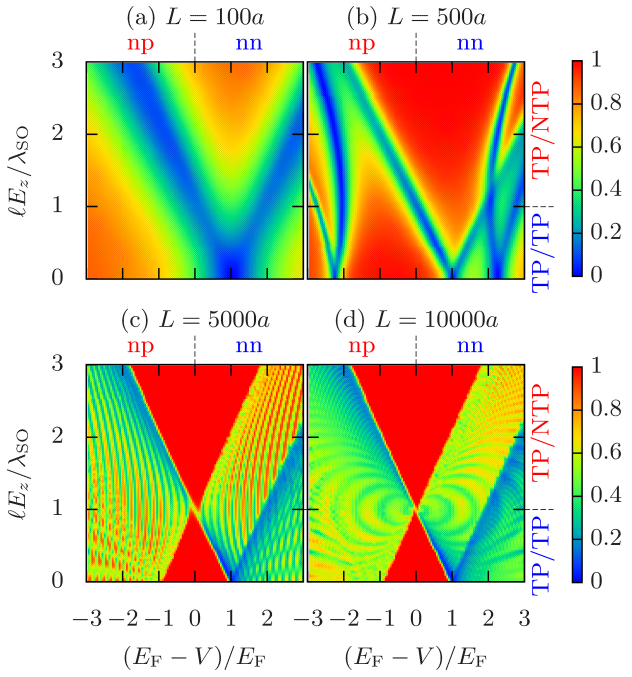

FIG. 12. Fano factor in the two-dimensional npn junction for $E_{\rm F} = 1.1\lambda_{\rm SO}$.

pression originates from matching/mismatching of the spin and sublattice states of the incident and transmitted electrons. Furthermore, the silicene pn junction has been shown to be a digital FET. It is not the case in the graphene pn junction, which has no band gap. The silicene junctions can be a potential new device controlled by two types of electric field V and E_z.

ACKNOWLEDGMENTS

This work is supported by the "Topological Quantum Phenomena" (No. 22103005) Grant-in Aid for Scientific Research on Innovative Areas from the Ministry of Education, Culture, Sports, Science and Technology (MEXT) of Japan. MH is supported by Grant-in Aid for Scientific Research No. 22740196.

Appendix A: Wave function in bulk silicene

The low-energy Hamiltonian Eq. (1) is rewritten as

$$H(\boldsymbol{k}) = v_{\rm F}(k_x\tau_x - k_y\tau_y\eta_z) + [\boldsymbol{g}(\boldsymbol{k})\cdot\boldsymbol{\sigma}\eta_z + \ell E_z]\,\tau_z, \tag{A1}$$

with $\boldsymbol{g}(\boldsymbol{k}) = (a\lambda_{\rm R}k_y, -a\lambda_{\rm R}k_x, -\lambda_{\rm SO})$. We diagonalize this Hamiltonian sequentially, i.e., diagonalizing the spin part (σ) in the first step and sublattice pseudo spin (τ) in the next step. The eigenvalue of $\boldsymbol{g}(\boldsymbol{k})\cdot\boldsymbol{s}$ is obtained to be $\pm g(\boldsymbol{k})$ with

$$g(\boldsymbol{k}) = \sqrt{g_x^2(\boldsymbol{k}) + g_y^2(\boldsymbol{k}) + g_z^2(\boldsymbol{k})} = \sqrt{a^2\lambda_{\rm R}^2k^2 + \lambda_{\rm SO}^2}. \tag{A2}$$

The corresponding eigenvector $|\boldsymbol{k}\pm\rangle_\sigma$ is given by

$$|\boldsymbol{k}\pm\rangle_s \propto [g_x(\boldsymbol{k}) - ig_y(\boldsymbol{k})]\,|\uparrow\rangle + [\pm g(\boldsymbol{k}) - g_z(\boldsymbol{k})]\,|\downarrow\rangle. \tag{A3}$$

As a result, the partially diagonalized Hamiltonian $H_\pm(\boldsymbol{k})$ is given by

$$H_\pm(\boldsymbol{k}) = v_{\rm F}(k_x\tau_x - k_y\tau_y\eta_z) + [\pm g(\boldsymbol{k})\eta_z + \ell E_z]\tau_z. \tag{A4}$$

Thus, the energy spectrum is obtained to be $\pm E_\pm(\boldsymbol{k})$ with

$$E_\pm^2(\boldsymbol{k}) = v_{\rm F}^2k^2 + [\pm g(\boldsymbol{k}) + \ell E_z]^2\,. \tag{A5}$$

The corresponding eigenvector $\boldsymbol{u}_\pm(\boldsymbol{k})$ is given by the direct product of the eigenvectors of the pseudo spin and the spin as

$$\boldsymbol{u}_\pm(\boldsymbol{k}) = |\boldsymbol{k}\pm\rangle_\tau|\boldsymbol{k}\pm\rangle_\sigma\,, \tag{A6}$$

with

$$|\boldsymbol{k}\pm\rangle_\tau \propto v_{\rm F}(k_x + ik_y\eta_z)\,|{\rm A}\rangle + [E_\pm(\boldsymbol{k}) - (\pm g(\boldsymbol{k})\eta_z + \ell E_z)]\,|{\rm B}\rangle\,. \tag{A7}$$

Appendix B: Symmetry

In this Appendix, we show the symmetry of the conductance in the silicene junction. Applying π-rotation along the x-axis, one obtains

$$\tau_x\sigma_xH(k_x,k_y)\sigma_x\tau_x = H(k_x,-k_y)|_{E_z\to -E_z}. \tag{B1}$$

The eigenvector $\boldsymbol{u}_\pm(\boldsymbol{k})$ is transformed as

$$\tau_x\sigma_x\boldsymbol{u}_\pm(k_x,k_y) = \boldsymbol{u}_\mp(k_x,-k_y). \tag{B2}$$

These lead to

$$r_{\alpha\beta} = r_{(-\alpha)(-\beta)}|_{k_y\to -k_y,E_z\to -E_z}. \tag{B3}$$

It follows that the charge conductance, which is obtained by the integral over k_y, α, and β, is an even function of E_z.

Next, we show the relation of the conductance between the two valleys. Applying unitary transformation $\tau_x\eta_x$, the Hamiltonian is transformed as

$$\tau_x\eta_xH(\boldsymbol{k})\tau_x\eta_x = H(\boldsymbol{k})|_{E_z\to -E_z}. \tag{B4}$$

The eigenvector is also transformed as

$$\tau_x\boldsymbol{u}_\pm(\boldsymbol{k}) = \boldsymbol{u}_\pm(\boldsymbol{k})|_{E_z\to -E_z,\eta_z\to -\eta_z}. \tag{B5}$$

From Eqs. (B3) and (B5), we conclude that the conductances contributed from K and K′ points are equivalent to each other.

[1] K. S. Novoselov, A. K. Geim, S. V. Morozov, D. Jiang, Y. Zhang, S. V. Dubonos, I. V. Grigorieva, and A. A. Firsov, Science **306**, 666 (2004).
[2] P. Vogt, P. De Padova, C. Quaresima, J. Avila, E. Frantzeskakis, M. C. Asensio, A. Resta, B. Ealet, and G. Le Lay, Phys. Rev. Lett. **108**, 155501 (2012).
[3] A. Fleurence, R. Friedlein, T. Ozaki, H. Kawai, Y. Wang, and Y. Yamada-Takamura, Phys. Rev. Lett. **108**, 245501 (2012).
[4] C.-L. Lin, R. Arafune, K. Kawahara, N. Tsukahara, E. Minamitani, Y. Kim, N. Takagi, and M. Kawai, Appl. Phys. Express **5**, 045802 (2012).
[5] C. L. Kane and E. J. Mele, Phys. Rev. Lett. **95**, 226801 (2005).
[6] C. L. Kane and E. J. Mele, Phys. Rev. Lett. **95**, 146802 (2005).
[7] H. Min, J. E. Hill, N. A. Sinitsyn, B. R. Sahu, L. Kleinman, and A. H. MacDonald, Phys. Rev. B **74**, 165310 (2006).
[8] Y. Yao, F. Ye, X.-L. Qi, S.-C. Zhang, and Z. Fang, Phys. Rev. B **75**, 041401 (2007).
[9] C.-C. Liu, W. Feng, and Y. Yao, Phys. Rev. Lett. **107**, 076802 (2011).
[10] K. Nomura, M. Koshino, and S. Ryu, Phys. Rev. Lett. **99**, 146806 (2007).
[11] S. Ryu, C. Mudry, H. Obuse, and A. Furusaki, Phys. Rev. Lett. **99**, 116601 (2007).
[12] O. Klein, Z. Phys. **53**, 157 (1929).
[13] M. I. Katsnelson, K. S. Novoselov, and A. K. Geim, Nat. Phys. **2**, 620 (2006).
[14] C. W. J. Beenakker, Rev. Mod. Phys. **80**, 1337 (2008).
[15] T. Ando, T. Nakanishi, and R. Saito, J. Phys. Soc. Jpn. **67**, 2857 (1998).
[16] B. Huard, J. A. Sulpizio, N. Stander, K. Todd, B. Yang, and D. Goldhaber-Gordon, Phys. Rev. Lett. **98**, 236803 (2007).
[17] M. Ezawa, New J. Phys. **14**, 033003 (2012).
[18] K. Takeda and K. Shiraishi, Phys. Rev. B **50**, 14916 (1994).
[19] T. Ohta, A. Bostwick, T. Seyller, K. Horn, and E. Rotenberg, Science **313**, 951 (2006).
[20] E. McCann and V. I. Fal'ko, Phys. Rev. Lett. **96**, 086805 (2006).
[21] E. McCann, Phys. Rev. B **74**, 161403 (2006).
[22] J. B. Oostinga, H. B. Heersche, X. Liu, A. F. Morpurgo, and L. M. K. Vandersypen, Nat. Mater. **7**, 151 (2008).
[23] Y. Zhang, T.-T. Tang, C. Girit, Z. Hao, M. C. Martin, A. Zettl, M. F. Crommie, Y. R. Shen, and F. Wang, Nature (London) **459**, 820 (2009).
[24] M. Ezawa, Phys. Rev. Lett. **109**, 055502 (2012).
[25] M. Ezawa, Phys. Rev. Lett. **110**, 026603 (2013).
[26] M. Ezawa, arXiv:1301.0971.
[27] M. Ezawa, arXiv:1303.1245.
[28] W.-F. Tsai, C.-Y. Huang, T.-R. Chang, H. Lin, H.-T. Jeng, and A. Bansil, Nat. Commun. **4**, 1500 (2013).
[29] C.-C. Liu, H. Jiang, and Y. Yao, Phys. Rev. B **84**, 195430 (2011).
[30] J. Cayssol, B. Huard, and D. Goldhaber-Gordon, Phys. Rev. B **79**, 075428 (2009).
[31] A. Yamakage, K.-I. Imura, J. Cayssol, and Y. Kuramoto, Europhys. Lett. **87**, 47005 (2009).
[32] A. Yamakage, K.-I. Imura, J. Cayssol, and Y. Kuramoto, Phys. Rev. B **83**, 125401 (2011).
[33] T. Yokoyama, Y. Tanaka, and N. Nagaosa, Phys. Rev. B **81**, 121401 (2010).